Model for Heterogeneous Catalysis on Metal Surfaces with Applications to Hypersonic Flows

M. Barbato* S. Reggiani†
CRS4 Research Centre – Cagliari, Italy

and

C. Bruno‡
Università di Roma I – Roma, Italy

J. Muylaert§
ESA-Estec, Noordwijk-The Netherlands

Abstract

A model for heterogeneous catalysis for Copper, Nickel, and Platinum has been devised. The model simulates the heterogeneous chemical kinetics of dissociated air flow impinging metal surfaces. Elementary phenomena such as, atomic and molecular adsorption, Eley-Rideal and Langmuir-Hinshelwood recombinations, and thermal desorptions have been accounted for. Comparisons with experimental results for Nitrogen and Oxygen recombination show good agreement.

In the second part of this work, the finite rate catalysis model has been used to analyze numerically the problems of heterogeneous catalysis similarity between hypersonic ground testing and reentry flight. Therefore the flow around a blunt cone under these conditions has been calculated and results for heat fluxes and for a suggested similarity parameter have been compared and discussed.

*Expert Research Engineer, CRS4 Research Centre, Sesta Strada Ovest, Zona Industriale Macchiareddu, P.O. Box 94, I-09010 Uta (CA) - Italy. Member AIAA.

†Aeronautical Engineer, formerly CRS4 fellow, presently at Andersen Consulting.

‡Associate Professor, Dipartimento di Meccanica e Aeronautica, Università di Roma I, Via Eudossiana 18, Roma 00184 - Italy, Senior Member AIAA.

§Head of Aerothermodynamics Section TOS-MPA. AIAA Member.

This article is a revised version of the AIAA Paper 96-1902, presented at the 31st AIAA Thermophysics Conference, June 17-20, 1996 - New Orleans, LA - USA.

Nomenclature

A	atom
$A*$	adsorbed atom = adatom
B_i	pre-exponential factor
d	atom diameter, m
D_{mi}	multidiffusion coefficient, m^2/s
E_i	activation energy, kJ/mole
E_{chem}	chemisorption energy, kJ/mole
h	Planck constant = $6.62608 \cdot 10^{-34}$ Js
k	Boltzmann constant = $1.38066 \cdot 10^{-23}$ J/K
k_i	rate constant, kg/m^2s
K_{wi}	catalyticity, m/s
L	body length, m
m	particle mass, kg
n	particle number density, particles/m^3
P_{0r}	Eley-Rideal microprobability
R	universal gas constant = 8.31451 J/mole K
s_{0a}	initial atomic sticking coefficient
s_{0m}	initial molecular sticking coefficient
t	time, s
T	translational-rotational temperature, K
T_V	vibrational-electronic temperature, K
x	body axis coordinate, m
Z_a	particles a flux, particle/m^2s
γ	recombination coefficient
ρ	mass density (kg/m^3)
θ	surface coverage
$[A]$	species A concentration, particles/m^3
$[AS]$	# of adatoms per unit area, particles/m^2
$[OS]$	# of O adatoms per unit area, particles/m^2
$[NS]$	# of N adatoms per unit area, particles/m^2
$[S]$	# of free sites per unit area, sites/m^2
$[S_0]$	# of sites per unit area, sites/m^2
$*$	active site
∞	free-stream value

Subscripts

a	atom
i	species i
m	molecule
$G-G$	atoms bond in a molecule
$G-M$	bond between atom and metal surface
ER	Eley-Rideal Mechanism
LH	Langmuir-Hinshelwood Mechanism
w	wall

Superscripts

G	gas phase

Introduction

Space vehicle reentry into the atmosphere and sustained hypersonic flight are technological challenges that have been driving aerospace research for several decades. The effort done in this field has been enormous and still continues, for example, by research programmes such as the Crew Rescue Vehicle (CRV: NASA X-38 programme).

This paper is meant as a contribution to the Thermal Protection System (TPS) problem. TPS must be reusable and allow the space vehicle to survive a hostile environment and ensure mission safety. TPS is as much necessary as it is heavy; therefore, TPS design optimization can lead to sensible vehicle weight reduction and to a possible vehicle payload increase.

A way to achieve this result is to obtain exact and reliable predictions for the vehicle thermal load during flight: the better we know it, the lighter the TPS could be. Therefore, the accurate simulation of the various processes contributing to the heat flux is a fundamental requirement. Heterogeneous catalysis is one of those processes and its importance has been already emphasized by several authors [1,2]. In fact, atomic species recombination on the vehicle surface leads to an additional heat flux entering the vehicles that can be up to 30% of the total heat load. Existing flight data about the catalytic activity of TPS coatings have been useful to understand the importance of this problem, but during design of new applications similar data are not available *a priori*. Ground tests can provide data, but the right coupling between hypersonic flow and surface catalytic efficiency should duplicate that in actual flight. This might not be possible if ground tests are performed by using "scaled down" models made of the same material used for TPS coatings. In fact, the catalytic activity of this class of coating material is purposely very low and it may be impossible to duplicate the ratio between the diffusive and the heterogeneous chemistry characteristic times when down-scaling the geometry by large factors. A possible solution is then to use models with a metal

skin which, due to its higher catalytic efficiency, may lead to close characteristic time ratios.

With this goal in mind, in this work a catalysis model for transition metals (Pt, Ni, Cu) interacting with O, N, O_2, N_2 will be presented. These metals have good catalytic efficiencies and have been selected because they are coatings candidate for wind tunnel test models. Also, to emphasize the similarity problem cited above, numerical simulations of the flow around a blunt cone in ground tests and flight conditions utilizing this model will be presented.

Physical Model

The heterogeneous catalysis process involving metal surfaces can be described by modeling its elementary steps. The kinetic model we assume is the following:

$$A^G + * \rightarrow A* \quad \text{chemisorption of atoms}$$

$$A_2^G + 2* \rightarrow A* + A* \quad \text{chemisorption of diatomic molecules}$$

$$A^G + A* \rightarrow A_2^G + * \quad \text{Eley-Rideal recombination}$$

$$A* + A* \rightarrow A_2^G + 2* \quad \text{Langmuir-Hinshelwood recombination}$$

$$A* \rightarrow A^G + * \quad \text{thermal desorption}$$

For each of these elementary steps a rate constant has been defined using an Arrhenius like expression[3]:

$$k_i = B_i e^{(-E_i/RT)} \tag{1}$$

where B_i is the frequency factor (the pre-exponential factor) and E_i is the activation energy, i.e., the amount of energy necessary to bring a mole of reacting molecule to the activated state. In

the following sections B_i and E_i will be defined at each step, to define the heterogeneous reaction mechanism.

Atom Adsorption

A gas atom reaching a metal surface interacts with it and is subject to attractive and repulsive forces. In fact, the surface atoms behave differently with respect to the bulk atoms for which there is a complete set of neighbors: on the surface there are unsaturated bonds that create "active sites" where the incoming atoms can be trapped forming a true chemical bond. An atom trapped in this way is called an adatom; the ratio between the number of adatoms and the number of available sites on the surface is called surface coverage.

For atoms such as O and N this adsorption process is spontaneous due to the large energy difference which exists between the two states: gas atom and adatom. For this reason atom adsorption can be assumed to be a non-activated process:

$$E_1 = 0 \quad \text{kJ/mole} \tag{2}$$

To set the pre-exponential factor we observe that the collision frequency (i.e., the number of collisions per unit area and unit time) of particles with a planar wall is [3]:

$$Z_c = n\sqrt{\frac{kT}{2\pi m}}$$

then the collision frequency at each site is:

$$Z_c' = n\sqrt{\frac{kT}{2\pi m}}\frac{1}{[S_0]} \quad .$$

Therefore, the velocity constant reads:

$$k_{coll} = \sqrt{\frac{kT}{2\pi m}}\frac{1}{[S_0]} \quad .$$

Clearly not all collisions are effective for adsorption, in fact:

- particles can reach the surface with an excess of energy that leads to a reflection;

- collision efficiency to adsorption depends on particle incident angle;

- vibrations of surface atoms can make adsorption more difficult;

- active site distribution on the surface is not uniform (steps, dislocations and other crystal irregularities may facilitate adsorption).

To account for the fact that only a percentage of atoms impinging the surface is adsorbed, we introduce an initial sticking coefficient s_{0a} defined as the probability of adsorption on a bare surface[i]. For the atomic initial sticking coefficient we assume the expressions:

$$s_{0a} = \overline{s}_{0a} \qquad \text{for} \quad T < T_{0a} \tag{3}$$

$$s_{0a} = \overline{s}_{0a} e^{(-\beta_a (T - T_{0a}))} \quad \text{for} \quad T \geq T_{0a} \tag{4}$$

where for temperatures lower than the threshold T_{0a}, the sticking coefficient is constant, whereas it decreases slightly with temperature above this threshold.

Finally, the rate constant for atomic adsorption reads:

$$k_1 = s_{0a} \cdot \sqrt{\frac{kT}{2\pi m_a}} \frac{1}{[S_0]} \quad . \tag{5}$$

[i] For particles as simple as atoms there are not steric effects. Therefore for atoms a unit steric factor can be assumed. On the contrary for complex molecules, adsorption may depend on the spatial arrangement of the molecules during the impact.

Molecule Adsorption

A molecule such as O_2 or N_2 can be adsorbed by a metal surface but only weakly bonded by van der Waals forces. This kind of adsorption is called physisorption and it may become important only at very low temperatures ($T < 154.8$ K for O_2 and $T < 126.1$ K for N_2)[4]. It may play a role as a precursor state for the dissociative chemisorption but does not have any influence on the surface coverage. Another possibility for molecular adsorption is the dissociative chemisorption: a molecule hitting the catalyst surface dissociates into two atoms that are adsorbed by two adjacent sites. What really happens it is that a molecule reaching the wall is first physisorbed and then dissociated (see Fig. 1). Dissociative chemisorption can be a "slightly activated" process because of the energy barrier between physisorbed molecules and chemisorbed atoms. This activation energy may be the reason for the slow chemisorption of gas molecules over certain surfaces (see Table 1 from Ref. 5). Following the same reasoning, we can assume a very small activation energy, or even the absence of activation energy for surfaces where chemisorption is fast. Therefore, looking at Table 1 for the metal surfaces considered in this work, we assume:

$$E_{m2} = 0 \quad \text{kJ/mole} \tag{6}$$

From the same table we see O_2 is adsorbed by all metals, except Au, which is not the case for N_2. A reason for this phenomenon can be found by observing that metals absorbing N_2 have free atoms with 3 or more vacancies in the d orbital whereas metals that do not adsorb N_2 the number of vacancies in the d orbital is lower than 3. Therefore, the high valence of N atoms may require at least 3 vacancies to allow adsorption.

Another reason for the difficult N_2 adsorption may be the site density, that is, the mean distance between adjacent sites. Suppose an atom of the N_2 molecule is close to a site: then, if the distance to the adjacent site is too great with respect to the molecule mean dimension, the second atom

is in an unfavorable position and dissociative adsorption becomes very difficult. Backing of this argument can be found in the lack of adsorption of N_2 on Pt, Pd and Rh, that all have a very large lattice parameter with respect to the N_2 dimensions. We also observe, however, that this argument notwithstanding, O_2 is adsorbed dissociatively on these metals. Therefore, besides geometric reasons, we suppose an influence of the difference between the energy for the atom-atom bond and the atom-metal bond: oxygen is strongly bonded to metal surfaces and also the energy E_{G-G} for O_2 is sensibly lower than for N_2. In conclusion, we assume O_2 can be chemisorbed by Pt, Cu and Ni, whereas N_2 cannot.

To define the rate constant of the dissociative adsorption of O_2 we start from the flux of molecules impinging a planar wall:

$$Z_m = n_m \sqrt{\frac{kT}{2\pi m_m}} \tag{7}$$

and we consider, as we did for atoms, an initial sticking coefficient, that we call the molecular sticking coefficient:

$$s_{0m} = \overline{s}_{0m} \qquad \text{for} \quad T < T_{0m} \tag{8}$$

$$s_{0m} = \overline{s}_{0m} e^{(-\beta_a (T - T_{0m}))} \quad \text{for} \quad T \geq T_{0m} \tag{9}$$

Also for this case, the sticking coefficient is constant for $T < T_{0m}$ and decreases slightly for $T > T_{0m}$. Experimental confirmation of this behavior is reported by Kisliuk[6] for N_2 on W. The same trend was found in the experiments of Melin and Madix[7] where $s_{0O_2} \sim 0.1 - 0.5$.

Finally, the rate constant for this elementary step is:

$$k_2 = s_{0m} \cdot \sqrt{\frac{kT}{2\pi m_m}} \frac{1}{[S_0]^2} \tag{10}$$

where the $[S_0]^2$ term is due to the fact that each dissociative adsorption needs two adjacent sites.

Eley-Rideal Recombination

Eley-Rideal (E-R) recombination occurs between a gas atom and an adatom: a gas atom reaching the metal surface hits an adatom and then recombines breaking the bond between adatom and surface. After recombination the molecule leaves the surface going back to the gas phase. The presence of this recombination mechanism was found by looking at the vibrational excitation of recombined molecules. In fact, studies[8] on H_2 formation over W show that the high vibrational excitation of molecules could not be justified by a recombination mechanism with high energy accomodation as, for example, Langmuir-Hinshelwood (see below).

The E-R recombination may be assumed as a non-activated process; in fact it is reasonable to assume that a gas atom, for example N, can extract an adatom from the surface without any extra energy supply, forming a bond stronger than that between the gas and the metal.

For O this picture is not reasonable when we deal with the high energy $O-M$ bond (e.g., for $O-W$ the bond energy is 672 kJ/mole). In this case we introduce an E-R micro-probability[9] useful to describe what our present ignorance of the details of this mechanism. In fact, to justify the E-R recombination for O atoms we can assume several scenarios:

- an E-R recombination may happen when the adatom is not yet at the bottom of the potential well, that is, it is not yet fully bonded to the metal surface;

- an E-R recombination may happen with adatoms in an excited state (energy may be supplied by catalyst lattice vibrational modes, i.e., phonons)[10];

- E-R recombination may involve O atoms not directly adsorbed by the metal but, for example, present above an oxide layer.

In any case, we expect this micro-probability to slightly increase with temperature. We assume, as already done for the sticking coefficients, a constant probability for temperatures lower than a

threshold, T_{0r}, and depending exponentially on T for higher temperatures:

$$P_{0r} = \overline{\alpha}_r \qquad \text{for } T < T_{0r} \tag{11}$$

$$P_{0r} = \overline{\alpha}_r e^{(\beta_r(T-T_{0r}))} \quad \text{for } T \geq T_{0r} \tag{12}$$

The derivation of the rate constant is similar to that of adsorption, with the only difference that P_{0r} replaces s_{0a}:

$$k_3 = P_{0r} \cdot \sqrt{\frac{kT}{2\pi m_a}} \frac{1}{[S_0]} \quad . \tag{13}$$

Langmuir-Hinshelwood Recombination

This mechanism of recombination is possible when atoms can move over the surface, that is, when they have enough energy to climb out of the potential well and migrate from one site to another. These moving atoms are still adsorbed, i.e., they do not leave the surface during migration; we assume they collide with the collisional frequency of a two-dimensional gas[11]:

$$B_4 = \sqrt{\frac{\pi kT}{2m_a}} d \quad . \tag{14}$$

The energy barrier that adatoms must overcome to migrate is the migration energy E_{mig} ($\sim 0.1 - 0.2$ of E_{chem} [11]), whereas to recombine they have to overcome a barrier given by:

$$E_{LH} = 2 \cdot E_{G-M} - E_{G-G} \quad . \tag{15}$$

Therefore, the activation energy for the Langmuir-Hinshelwood (L-H) recombination is the higher between E_{LH} and E_{mig}. For the surfaces and the molecules considered in this work it is always $E_{LH} > E_{mig}$. Therefore, we assume $E_4 = E_{LH}$. Finally, for L-H recombination, the rate constant reads:

$$k_4 = \sqrt{\frac{\pi kT}{2m_a}} d \cdot e^{(-E_4/RT)} \quad . \tag{16}$$

Thermal Desorption

If an adatom acquires enough energy, it may vibrate to the point of breaking the bond $G-M$ and then it may leave the surface without recombining. This process is called thermal desorption. Thermal desorption is clearly an activated process; there are in fact applications of catalysis where thermal desorption is programmed for a well defined temperature[12]. For the activation energy of this elementary process we assume:

$$E_5 = E_{G-M} \quad . \tag{17}$$

Due to the high values of E_5, thermal desorption becomes important at very high temperatures (e.g., $T > 2000$ K for N adsorbed on W [9]). To define the rate constant we assume the frequency factor equal to the vibration frequency[13]:

$$B_5 = \frac{kT}{h} \tag{18}$$

Finally, for Thermal Desorption, we write the rate constant as:

$$k_5 = \frac{kT}{h} \cdot e^{(-E_5/RT)} \quad . \tag{19}$$

Surface Coverage

Over a metal surface invested by a flow of atoms and molecules, all of these elementary processes act simultaneously. After a transient, the surface coverage reaches a steady state condition:

$$\frac{d[AS]}{dt} = 0$$

Applying this condition, by taking into account all of the elementary processes, we obtain a second order equation for the adatom density $[AS]$:

$$k_1[A][S] + 2k_2[A_2][S]^2 - k_3[A][AS] - 2k_4[AS]^2 - k_5[AS] = 0 \tag{20}$$

where $[S] = [S_0] - [AS]$ is the number of free sites per unit area. Using this last expression in Eq. (20), we have:

$$a[AS]^2 + b[AS] + c = 0 \tag{21}$$

where

$$a = 2k_2[A_2] - 2k_4 \tag{22}$$

$$b = -k_1[A] - 4k_2[A_2][S_0] - k_3[A] - k_5 \tag{23}$$

$$c = k_1[A][S_0] + 2k_2[A_2][S_0]^2 \tag{24}$$

As can be seen the signs of b and c are well defined ($b < 0$ and $c > 0$) whereas the sign for a is not obvious. The two solutions of Eq. (21) are:

$$[AS] = \frac{-b \pm \sqrt{b^2 - 4ac}}{2a} \tag{25}$$

but only one of those has physical meaning. To find the right physical solution, we examine the two possible cases for a:

$a < 0$ one of the solutions is negative. We take the positive one;

$a > 0$ in this case both solutions are positive but only one is an equilibrium solution.

For both of these cases the correct physical solution is:

$$[AS] = \frac{-b - \sqrt{b^2 - 4ac}}{2a} \tag{26}$$

Finally surface coverage is:

$$\theta = \frac{[AS]}{[S_0]} \quad . \tag{27}$$

Recombination Coefficient

The atomic recombination coefficient is defined as[14]:

$$\gamma = \frac{\text{flux of atoms recombining at surface}}{\text{flux of atoms impinging the surface}}$$

To calculate γ, we start from the number of molecules formed per unit area and unit time:

$$\frac{d[A_2]}{dt} = -k_2[A_2][S]^2 + k_3[A][AS] + k_4[AS]^2 \tag{28}$$

then, the rate of atom consumption at the wall is:

$$-\frac{d[A]}{dt} = 2 \cdot \frac{d[A_2]}{dt} = 2 \cdot (-k_2[A_2][S]^2 + k_3[A][AS] + k_4[AS]^2). \tag{29}$$

Therefore:

$$\gamma = \frac{2 \cdot (-k_2[A_2][S]^2 + k_3[A][AS] + k_4[AS]^2)}{Z_a} \tag{30}$$

and γ is a function of T and of A and A_2 partial pressures. Once the surface coverage θ is known, we can calculate the recombination coefficient.

O and N simultaneous recombination

When both O and N atoms reach the catalyst surface, (e.g. in the case of a hypersonic flow past a body), both can adsorb. Therefore the number of free sites per unit area will be[15,16,17]:

$$[S] = [S_0] - [OS] - [NS] \tag{31}$$

because there is competition in occupying the sites.

At steady state, to determine the surface coverage we must write an equation for each atomic species. Therefore, by proceeding as done for Eq. 20, we obtain the system:

$$a_1[OS]^2 + b_1[NS]^2 + c_1[OS][NS] + d_1[OS] + e_1[NS] + f_1 = 0 \tag{32}$$

$$a_2[OS]^2 + b_2[NS]^2 + c_2[OS][NS] + d_2[OS] + e_2[NS] + f_2 = 0 \tag{33}$$

where the two equations are coupled. The solutions of this system are the O and N surface coverages.

Once these quantities are known, we can calculate the two recombination coefficients for the simultaneous formation of O_2 and N_2:

$$\gamma_{OO} = \frac{2 \cdot (-k_2[O_2][S]^2 + k_3[O][OS] + k_4[OS]^2)}{Z_O} \tag{34}$$

$$\gamma_{NN} = \frac{2 \cdot (-k_2[N_2][S]^2 + k_3[N][NS] + k_4[NS]^2)}{Z_N} \tag{35}$$

Both γOO and γNN are lower than those obtained for a pure oxygen or for a pure nitrogen flow. In fact, even if temperatures and partial pressures are the same, competitive adsorption reduces the recombination probabilities of both species. The possibility to have cross recombination with formation of NO molecules, accounted for by other authors[18], is not considered in this work but it can be a further development of this model.

Parameter Definition

The coefficients $\overline{s}_{0a}$, β_a, T_{0a}, $\overline{s}_{0m}$, β_m, T_{0m}, $\overline{\alpha}_r$, β_r, T_{0r}, E_4, and E_5, have been based upon experimental data available in literature. Nitrogen adsorption and recombination data exist for temperatures up to the melting point of many materials, but for Oxygen most available data are scattered at temperatures near ambient. This fact has been one of the major problems in picking numbers for the Oxygen related parameters.

The approach followed to define the parameters can be summarized in three steps:

1. define a range of variation for each coefficient (fix "margins"). This was done using the data available in literature or applying physical constraints.

2. Define a set of experimental values for the recombination coefficient useful as targets in a parameter optimization procedure. These data were obtained from a literature search[5,6,14,19].

3. Define "best" value for each coefficient. This was done by implementing a least square procedure to define the value for each coefficient imposing: a) the range of variation of step 1; b)

the minimum difference between the calculated and experimental values of step 2.

Experience gained in determining the Nitrogen coefficients was used to define the parameters for Oxygen recombination when data were not available. In particular, the data taken from Ref. 9 on metals such as Pd, Re, Ta, Rh where analyzed to infer a possible common behavior for the transition metals when they act as catalysts in recombination phenomena. The results of this analysis led to the following observations:

- starting from ambient temperature, the recombination coefficient has a low value nearly constant with temperature;
- after a certain temperature threshold T_{wt}, the recombination coefficient rises sharply;
- at very high temperature ($T_w \gg T_{wt}$) the recombination coefficient tends slowly to a maximum.

This "S" curve type, shown by almost all of the metal surfaces, can be explained looking at the processes involved in the heterogeneous recombination[20]. The first part of the γ trend is characterized by recombination mainly due to the E-R mechanism. In fact, at low temperatures ($T_w \ll T_{wt}$), the surface coverage is high (~ 1) because thermal desorption is negligible and the L-H mechanism is not yet activated. This leads to a very high probability that gas atoms may strike adsorbed ones.

This behavior does not change with T_w until the L-H desorption starts being activated. At that point ($T_w \sim T_{wt}$), there is a steep increase in the recombination coefficient and a simultaneous reduction of the surface coverage. In fact, the L-H mechanism is very efficient in removing atoms, for each recombination two adatoms are extracted from the surface. Under these conditions the E-R mechanism becomes less and less efficient, because for it becomes more and more unlikely that a gas atom may strike an adatom.

Raising T_w even higher ($T_w > T_{wt}$), thermal desorption becomes important, further reducing the number of adatoms and therefore the recombination probability. Besides, the reduction of the sticking coefficient leads to a further decrease of adsorption efficiency and thus surface coverage. Finally, when the metal temperature is near to its melting point, T_f, we can also envisage a reduction of the recombination coefficient due also to the solubilization of adsorbed species into the bulk. Based on this discussion, available experimental data, physical constraints and macroscopical trend, the *a priori* unknown parameters were determined in a wide range of temperatures ($300K - T_f$). The set of parameters for Oxygen and Nitrogen is shown in Table 2.

Model Accuracy

The accuracy of the model presented here is greatly dependent on the quantity of experimental data available. The availability of experimental data, especially in the temperature region where the γ curve changes slope, can make the difference between the quantitative and the qualitative effectiveness of the model. Even just one experimental point can be crucial as, for example, Fig. 8 shows. Therefore the authors, even though the details of the chemico-physical model are the same, would consider much more accurate γs for N on W and on Pt and for O on Pt than the other recombination coefficients presented here which, instead, should be considered only qualitatively reliable.

Catalysis Model: Results

Nitrogen Recombination

The recombination coefficient γ_{NN} predicted by this model is shown as a function of T in Figs. 2-5. The N and N_2 partial pressures used for these test cases are from Ref. 9. The γ behavior already announced above (S-curve) is evident. For all the surfaces considered, the sticking coefficient is

quite high (~ 0.5) and it decreases slowly with temperature. This means that N adsorption is a very efficient process, leading to an high surface coverage (notice that there is not N_2 chemisorption). This implies the E-R mechanism is very effective at low temperatures. This last conclusion is also due to the large difference that exist between E_{G-G} and E_{G-M}.

When the experimental data are available over a wide range of temperatures, we can see that the model reproduces qualitatively and quantitatively well the data. For metal as Ni and Cu we expect the model to be qualitatively correct but we need more experimental data over a wider range of temperature to state quantitative conclusions.

Oxygen Recombination

The results obtained for Oxygen recombination are presented in Figs. 6-8. All these results are for non-oxidized surfaces. In fact, accounting for the presence of an oxide layer leads to very complex issues: e.g., which oxide is stable at a certain temperature, and which are the parameters for each oxide. This already difficult problem is further complicated by the unavailability of data specifying the actual degree of oxidation of surfaces used as samples. Therefore, making this assumption, we predict recombination coefficients γ_{OO} that may be higher than those relative to oxides.

For Cu and Ni all the experimental data available are at ambient temperature, and the γ_{OO} values at higher T have been inferred as explained above. Results for Pt show good agreement with experiments. In particular, going from low to medium temperatures, the γ_{OO} change in slope due to the L-H mechanism activation is well reproduced.

Based on these results we can say that the model predicts qualitatively well the recombination coefficient behavior in a wide range of temperatures. At the moment, no accurate quantitative conclusions can be drawn.

Flow Simulation Results

The finite rate catalysis model presented in the first part of this work has been implemented in an hypersonic flow solver (TINA [24]) to simulate the catalytic activity over the skin of a body in a hypersonic airflow.

The blunt body solution use free stream conditions reproducing: 1) the flow in the test chamber of the T5 piston shock tunnel[21] (with $P_0 = 18$ MPa, and $H_0 = 20$ MJ/Kg reservoir conditions) and 2) flight at 40 km altitude (see Table 3). Numerical simulations of these conditions are then compared to analyze the possibility to duplicate in a wind tunnel test the coupling between hypersonic flow and heterogeneous catalysis found in flight.

Body geometry, code and numerical tests description

The model shape is a 33.0 cm long sphere/cone with a 2.916 cm nose radius and a 4.66 degree half-cone angle, representing the reentry capsule ELECTRE[23] in 1/6 scale. The hypersonic flow past the blunt cone was solved by the 3D Navier-Stokes solver TINA[24] assuming a thin layer approximation for a 5-species gas with a two-temperature model (T, T_V). The catalytic boundary condition are implemented following the approach of Ref. 25. The wall is supposed to be isothermal and thermal equilibrium is imposed $((T_V)_w = (T)_w = T_w)$. This latter conditions implies that for the catalytic cases, recombined molecules, deposit their extra energy on the surface, reaching complete energy accomodation before desorbing (thermal and chemical energy accomodation factor[9] $\beta = 1$)

Heat Flux Results

Several numerical simulations of the flow around ELECTRE, with T5 wind tunnel free stream conditions and different coating materials, have been performed at $T_w = 500$ K. Beside the finite rate catalysis model, Non-Catalytic (NC: $\gamma = 0$) and Fully-Catalytic (FC: $\gamma = 1$) boundary conditions have also been implemented. Figure 9 shows the calculated total heat fluxes; the highest values are obtained by using a FC condition, whereas the minimum values belong to the NC case. Heat fluxes for the model with a metal surface are between these two cases. We can see that for metal surfaces the higher heat flux is obtained using Cu, followed by Ni and Pt. Figure 10 shows the diffusive contributions for each catalytic case, giving again $FC > Cu > Ni > Pt$.

As for the translational and vibrational heat flux contributions, their behavior is exactly reversed, i.e., $NC > Pt > Ni > Cu > FC$ (see Fig. 9). This is due to the complete energy accomodation condition that forces the recombined molecules to desorb in thermal equilibrium with the wall leading to a "catalytic cooling effect[26]." In fact, the flux of recombined molecules cools the layer of gas near to the wall, reducing the amount of conductive heat flux. Clearly when this flux is zero, i.e., for a

non catalytic wall, the conductive contribution to total heat flux is maximum.

A comparison between numerical simulation of the ground test flow in T5 and the experimental results of Ref. 21 is shown in Fig. 11. The model surface temperature is 300 K and the catalytic activity of its stainless steel surface has been simulated using Ni in the catalysis model.

The heat flux trend has been reproduced except on the body nose, where it is somewhat lower. Better agreement is obtained on the conical part of the body.

The Similarity Problem: Results

The question we asked is, whether the coupling between gas flow and surface catalytic activity found in flight can be reproduced in a wind tunnel. The similarity parameter we introduce (from the species boundary conditions) is the ratio between the diffusion and the heterogeneous chemistry characteristic times:

$$Da_w = \frac{\tau_{df}}{\tau_{cw}} \tag{36}$$

that is, for the chemical species i

$$Da_{wi} = \frac{K_{wi} Y_i}{\mathcal{D}_{mi} (\nabla Y_i)_w} \tag{37}$$

where the catalyticity for the species i reads[14]:

$$K_{wi} = \gamma \sqrt{\frac{kT_w}{2\pi m_s}} \quad . \tag{38}$$

Due to the analogy with the Damköhler number, we call this parameter the "heterogeneous Damköhler number". Its value characterizes the heterogeneous chemistry-diffusion coupling: when $Da_w \gg 1$, catalysis is controlled by diffusion (wall recombinations are so fast that they are limited by the flux of incoming atoms); when $Da_w \ll 1$, catalysis is slow with respect to diffusion and catalytic activity becomes a secondary effect. Due to the dominance of heterogeneous recombination of oxygen during atmospheric reentry, we begin by assuming Da_{wO} as the relevant similarity parameter.

A comparison between Da_{wO} in flight and in the wind tunnel has been performed (see Fig. 12): ELECTRE in flight has been assumed coated with Silica, that is representative of the catalytic behavior of the Reaction Cured Glass used as a TPS coating[27]. The Silica catalytic behavior has been simulated by using the model of Nasuti et al.[18] but excluding, for simplicity, NO surface reactions. The free stream conditions for the flight case are those corresponding to the point at ~ 293 sec. of the ELECTRE trajectory during its first experimental flight[28] (see Table 3).

The wind tunnel (WT) results for a Silica surface are qualitatively different from those in flight: on the nose, Da_{wO} is lower and does not show the maximum found in flight; besides, on the cone Da_{wO} increases much more than in flight. The WT results obtained with a metal skin are instead closer to those in flight especially on the nose, where they show a maximum at the same location. The values of Da_{wO} over the cone have a different slope but are closer to the flight values than in the case of WT-Silica results.

The best agreement on the nose is obtained coating the surface with Pt. This interesting result must be carefully considered because the Da_{wN} produced in WT by using a metal skin differs substantially by the value in flight (see Fig. 13). This is due to the high catalytic efficiency of metals for N recombination at relatively low temperatures (O is too strongly bonded by metals, and at these temperatures its catalytic recombination is less efficient, see Figs. 3-8). The influence of this result on the effectiveness of the similitude criteria envisaged in this work should be of secondary importance (compare Figs. 12 and 13) due to the very small quantity of atomic nitrogen that reaches the surface, under the testing conditions assumed, but needs further investigation.

A comparison between heat fluxes in WT and in flight is displayed in Fig. 14. The WT curves show the heat transfer to be larger than in flight; the trend is very similar on the nose but shows a different slope on the cone. This is due, in part, to the difference in temperature in this zone of the body; in flight, temperatures near the body surface are lower than in WT, due to the free stream

characteristics and to the larger body length that allow the gas flow to cool more. In fact, Fig. 15 shows that translational temperature gradients normal to the wall have a similar slope difference. This difference has also been found for the diffusive heat fluxes (see Fig. 16), suggesting the WT does not reproduce well flight catalysis, at least over this part of the body (see also the results for Da_{wO} in Fig. 12).

In conclusion, the WT and flight heat fluxes trends seem to be quite similar on the body nose, whereas they differ on the cone. This suggests that similarity between WT and flight data has to be considered more carefully over the cone. Therefore, future work will define a suitable "scaling law" to correlate these results.

Conclusions

The finite rate catalysis model presented here simulates the catalytic activity of metal surfaces (Cu, Ni, Pt) in a dissociated gas (N_2, O_2, and air) flow. Comparison of our results with experimental data shows good agreement. Where experimental data were not available, the catalytic behavior has been inferred from similar results for other transition metals and from results obtained with the same metal but with other gas species.

This finite rate catalysis model has been implemented in a Navier-Stokes solver to calculate an hypersonic flow past a blunt body taking into account the catalytic effects due to a metallic skin. Calculated results lie between the results for the two extreme cases: Fully-Catalytic and Non-Catalytic.

The possibility to duplicate in-flight-TPS catalytic activity by metal coated models in ground tests has been explored. Using Da_{wO} as parameter shows this can be successfully accomplished especially on the body nose, whereas on the cone quantitative and qualitative differences exist. The high catalytic activity of recombining nitrogen leads instead to Da_{wN} differences between flight and

wind tunnel data. Further analysis will define a scaling law to correlate wind tunnel and flight data and will check the influence that the Da_{wN} difference could have.

Acknowledgments

The authors gratefully acknowledge the CRS4 Research Centre for the financial support to Dr. S. Reggiani during her two month stage. This work has been carried out with the financial support of the Sardinian Regional Government.

References

[1] Scott, C.D., "Catalytic Recombination of Nitrogen and Oxygen on High-Temperature Reusable Surface Insulation," *Aerothermodynamics and Planetary Entry*, edited by A.L. Crosbie, Progress in Astronautics and Aeronautics, AIAA, New York, 1980, pp. 193-212.

[2] Stewart, D.A., Rakich, J.V. and Lanfranco, M.J., "Catalytic Surface Effects Experiment on the Space Shuttle," *Thermophysics of Atmospheric Entry*, edited by T.E. Horton, Vol. 82, Progress in Astronautics and Aeronautics, AIAA, New York, 1982, pp. 248-272.

[3] Yeremin, E.N., *The Foundations of Chemical Kinetics*, 1979, MIR Publisher, Moscow.

[4] Silvestroni, P., *Fondamenti di chimica*, 1982, Libreria Eredi Virgilio Veschi, Roma.

[5] Hayward, D.O. and Trapnell, B.M.W., *Chemisorption*, 1964, Butterworths, London.

[6] Kisliuk, P., "The Sticking Probabilities of Gases Chemisorbed on the Surfaces of Solids", *Journal of Physical Chemistry, Solids*, Vol.3, 1957, pp. 95-101.

[7] Melin, G.A. and Madix, R.J., "Energy Accomodation During Oxygen Atom Recombination on Metal Surfaces", *Transactions Faraday Society*, Vol.67, No.1, 1971, pp. 198-211.

[8] Kratzer, P. and Brenig, W., "Highly Excited Molecules from Eley-Rideal Reactions", *Surface Science*, Vol.254, 1991, pp. 275-280.

[9] Halpern, B. and Rosner, D.E., "Chemical Energy Accomodation at Catalyst Surfaces", *Chemical Society, Faraday Transactions I*, Vol.74, 1978, pp. 1833-1912.

[10] Bond, G.C., "Source of the Activation Energy in Heterogeneously Catalysed Reactions", *Catalysis Today*, Vol.17, 1993, pp. 399-410.

[11] Tompkins, F.C., *Chemisorption of Gases on Metals*, 1978, Academic Press, London.

[12] Delgass, W.N. and Wolf, E.E., "Catalytic Surfaces and Catalyst Characterization Method", in *Chemical Reaction and Reactor Engineering*, Carberry J.J. and Varma A. editors, 1987, Marcel Dekker, New York.

[13] Bamford, C.H., *Comprehensive Chemical Kinetics*, 1969, Elsevier, Amsterdam.

[14] Scott, C.D., "Wall Catalytic Recombination and Boundary Conditions in Nonequilibrium Hypersonic Flows - with Applications", in *Advances in Hypersonics Vol. 2*, Bertin J.J., Periaux J., Ballmann J. editors, 1992, Birkhäuser, Boston, pp. 176-249.

[15] Jumper, E.J., Ultee, C.J. and Dorko, E.A., "A Model for Fluorine Atom Recombination on a Nickel Surface", *J. of Physical Chemistry*, Vol.84, 1980, pp. 41-50.

[16] Seward, W.A., and Jumper E.J., "Model for Oxygen Recombination on Silicon-Dioxide Surfaces", *J. of Thermophysics and Heat Transfer*, Vol.5, No.3, 1991, pp. 284-291.

[17] Jumper E.J., Newman, M., Kitchen, D.R. and Seward, W.A., "Recombination of Nitrogen on Silica-Based Thermal-Protection-Tile-Like Surfaces", AIAA Paper 93-0477, Jan. 1993.

[18] Nasuti, F., Barbato, M. and Bruno, C., "Material-Dependent Catalytic Recombination Modeling for Hypersonic Flows", *J. of Thermophysics and Heat Transfer*, Vol.10, No.1, 1996, pp. 131-136.

[19] Greaves, J.C. and Linnett, J.W., "The Recombination of Oxygen Atoms at Surfaces", *Transactions Faraday Society*, Vol.54, 1958, pp. 1323-1330.

[20] Barbato, M. and Bruno, C., "Heterogeneous Catalysis: Theory, Models and Applications", in *Molecular Physics and Hypersonic Flows*, Capitelli M. editor, NATO-ASI Series C, Vol. 482, 1996, Kluwer Academic Publisher, Dordrecht, pp. 139-160.

[21] Rousset, B. and Adam, P., "Electre Experiments in T5", Graduate Aeronautical Laboratories California Institute of Technology FM 93-2, September 1993.

[22] Bellucci, V., Ueda, S., Eitelberg, G. and Muylaert, J., "Experimental and Numerical Analysis of a Blunt Body Configuration in T5 and HEG", in *Second European Symposium on Aerothermodynamics for Space Vehicles*, November, 1994 ESA-ESTEC Noordwijk, The Netherlands, European Space Agency Publisher.

[23] Muylaert, J., Walpot, L.M.G., and Durand, G., "Computational Analysis on Generic Forms in European Hypersonic Facilities: Standard Model Electre and Hyperboloid-Flare", in *Shock Waves at Marseille*, R. Brun and L.Z. Dumitrescu editors, 1995, Springer-Verlag, Berlin, pp. 19-28.

[24] Netterfield, M.P., "Validation of a Navier-Stokes Code for Thermochemical Non-Equilibrium Flows", AIAA Paper 92-2878, July 1992.

[25] Barbato, M., Giordano, D. and Bruno, C., "Comparison Between Finite Rate and Other Catalytic Boundary Conditions For Hypersonic Flows", AIAA Paper 94-2074, June 1994.

[26] Barbato, M., Giordano, D., Bruno, C. and Muylaert, J., "Catalytic Wall Condition Comparisons for Hypersonic Flow", *J. of Spacecraft and Rockets*, Vol.33, No.5, Sept.-Oct. 1996, pp. 620-627.

[27] Carleton, K.L. and Marinelli, W.J., "Spacecraft Thermal Energy Accomodation from Atomic Recombination", *J. of Thermophysics and Heat Transfer*, Vol.6, No.4, 1992, pp. 650-655.

[28] Muylaert, J., Walpot, L., Häuser, J., Sagnier, P., Devezeaux, D., Papirnyk, O., and Lourme, D., "Standard Model Testing in the European High Enthalpy Facility F4 and Extrapolation to Flight", AIAA Paper 92-3905, July 1992.

List of Figures

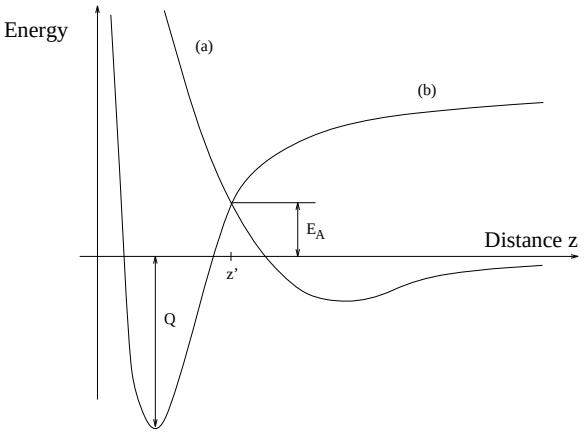

Figure 1: Potential energy curves for adsorption: (a) physisorption of a molecule; (b) chemisorption of two atoms. From Ref. 20

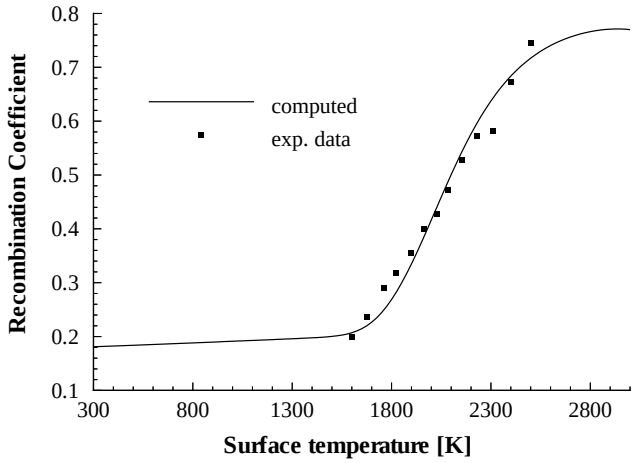

Figure 2: Nitrogen recombination on W: comparison between model results and experiments of Ref. 9.

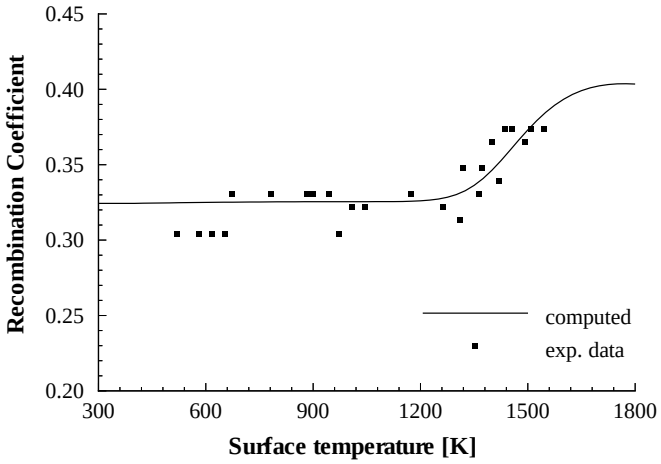

Figure 3: Nitrogen recombination on Pt: comparison between model results and experiments of Ref. 9.

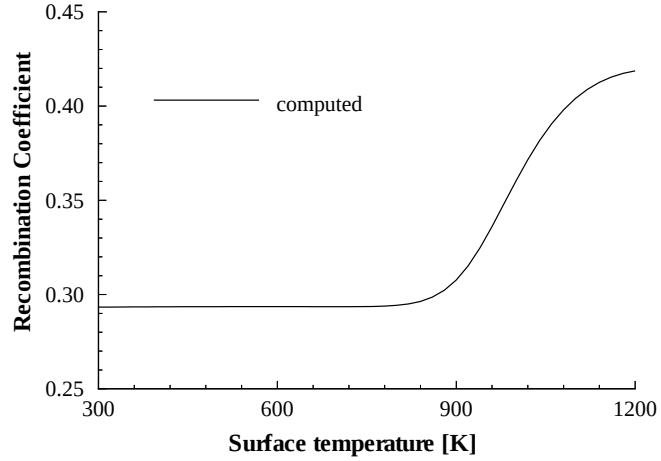

Figure 4: Nitrogen recombination on Cu.

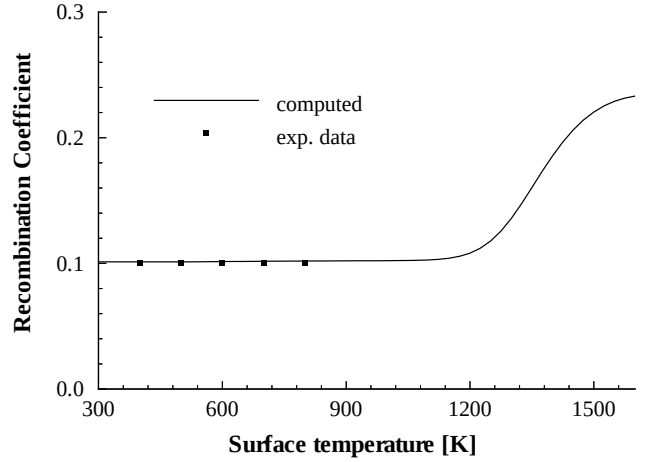

Figure 5: Nitrogen recombination on Ni: comparison between model results and experimental data.

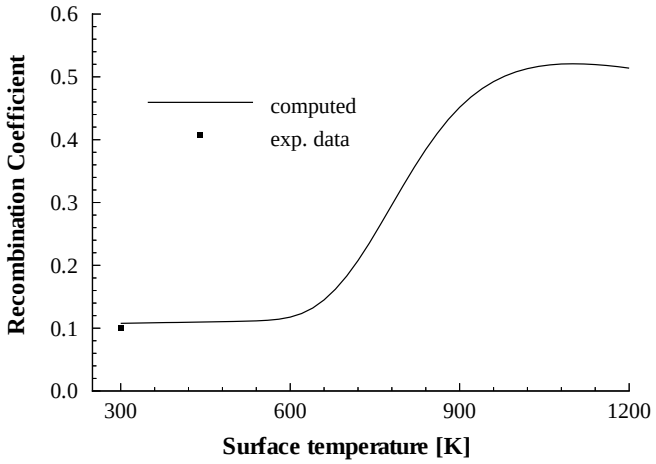

Figure 6: Oxygen recombination on Cu: comparison between model results and experimental data.

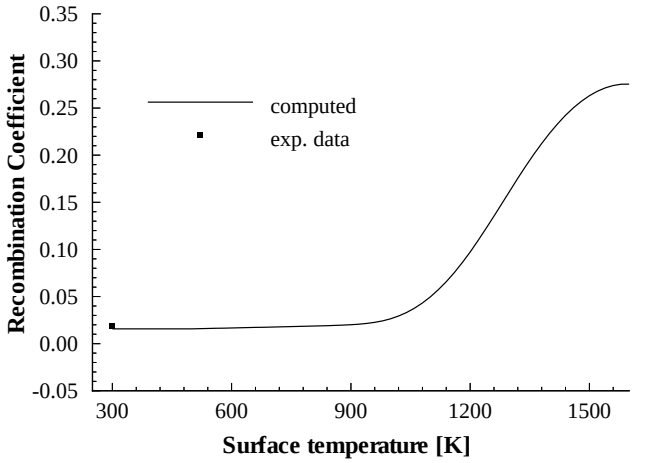

Figure 7: Oxygen recombination on Ni: comparison between model results and experimental data.

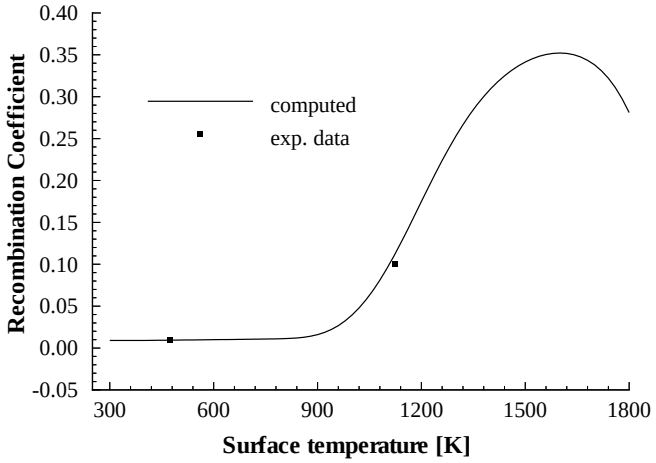

Figure 8: Oxygen recombination on Pt: comparison between model results and experimental data.

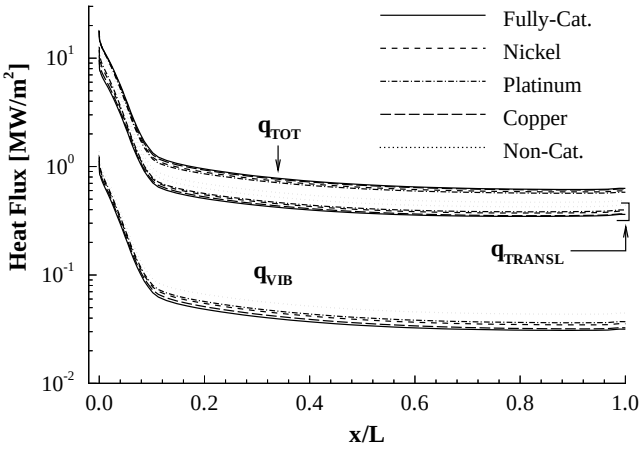

Figure 9: Surface heat fluxes (T_{wall} = 500 K): conductive contributions (translational and vibrational) and total heat flux.

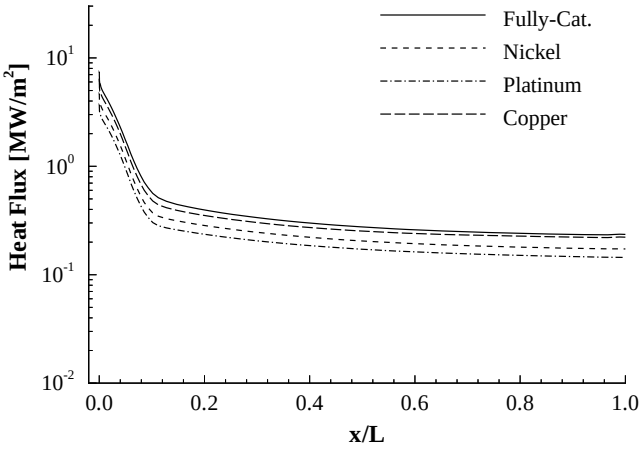

Figure 10: Surface heat fluxes (T_{wall} = 500 K): diffusive contribution.

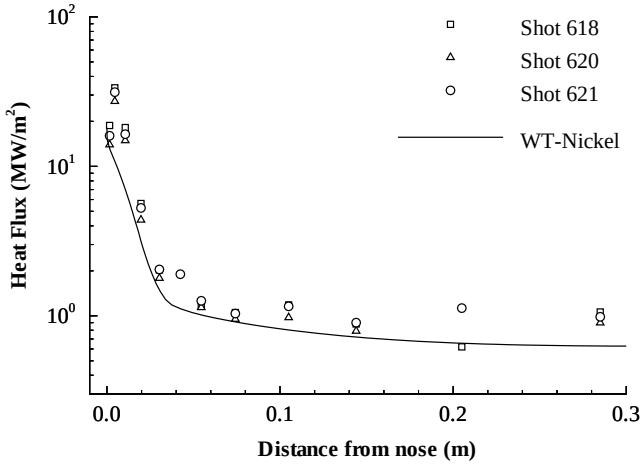

Figure 11: Surface heat fluxes (T_{wall} = 300 K): comparison with experimental data from Ref. 21.

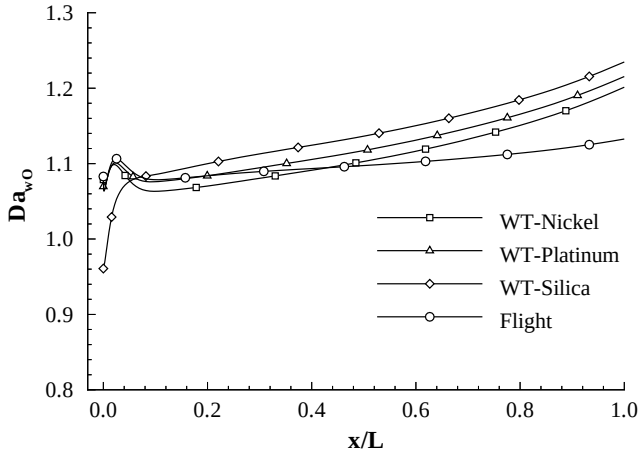

Figure 12: Damköhler number comparison for Oxygen ($T_w = 800$ K).

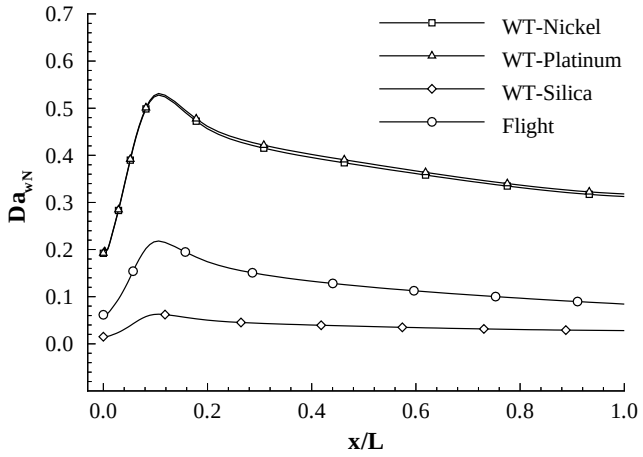

Figure 13: Damköhler number comparison for Nitrogen ($T_w = 800$ K).

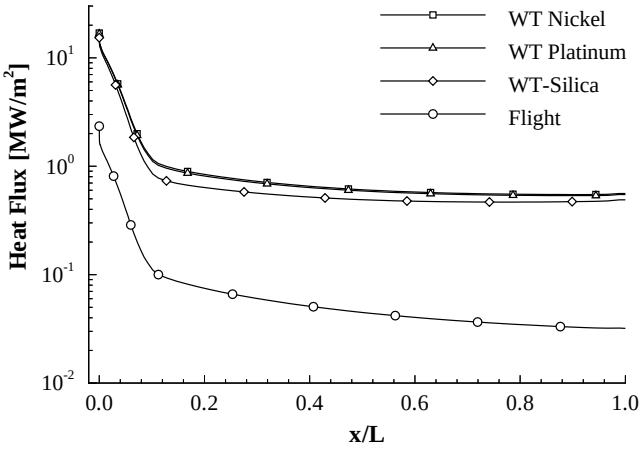

Figure 14: Total heat flux: comparison between wind tunnel and flight simulations ($T_w = 800$ K).

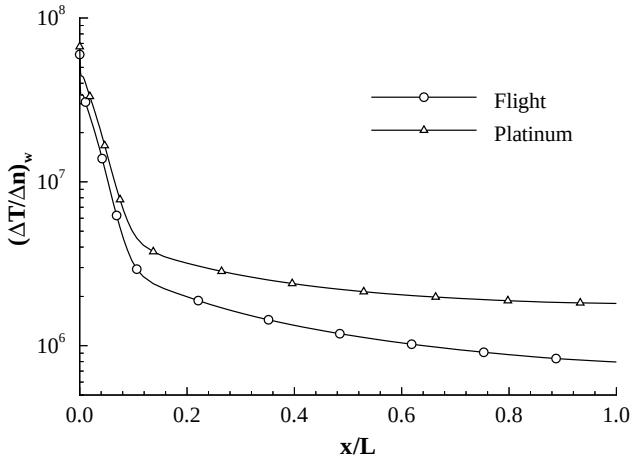

Figure 15: Comparison between wind tunnel and flight temperature gradient normal to the body surface ($T_w = 800$ K).

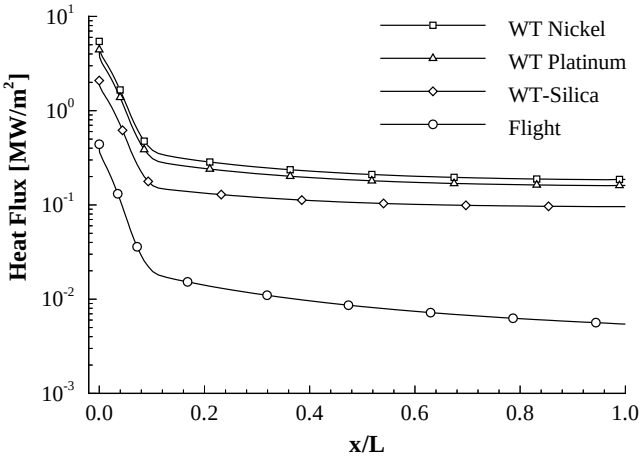

Figure 16: Diffusive heat flux: comparison between wind tunnel and flight simulations ($T_w = 800$ K).

Table 1: Chemisorption on Metal Films. From Ref. 27

Gas	Very fast chemisorption	Slow chemisorption	No chemisorption up to O° C
H_2	Ti, Zr, Nb, Ta, Cr Mo, W, Fe, Co, Ni Rh, Pd, Pt, Ba	Mn, $?Ca$, Ge	K, Cu, Ag, Zn Cd, Al, In, Pb, Sn
O_2	All metals except Au	$--$	Au
N_2	La, Ti, Zr, Nb, Ta	Fe, $?Ca$, Ba	As for H_2 plus Ni, Rh, Pd, Pt

Table 2: Model Parameters.

	Metal	$[S_0]$	$\overline{s}_{0a}$	β_a	T_{0a}	$\overline{s}_{0m}$	β_m	T_{0m}	$\overline{\alpha}_r$	β_r	T_{0r}	E_4	E_5
N_2	W	1.35	.825	.00001	650	.29	.0005	475	.15	.00005	500	330	637.5
	Pt	1.25	.55	.0002	400	-	-	-	.23	.0001	400	265	605
	Ni	1.54	.45	.0005	500	-	-	-	.057	.000095	500	260	602.5
	Cu	1.47	.55	.00025	300	-	-	-	0.2	.0001	300	175	560
O_2	Pt	1.25	.45	.0001	400	.2	.0005	400	.0055	.0005	400	190	344
	Ni	1.54	.6	.0005	500	.3	.0005	500	.01	.0007	500	210	354
	Cu	1.47	.8	.00045	300	.4	.0006	300	.085	.0002	300	120	309

Table 3: Free stream conditions for flight and wind tunnel (WT) simulations. Wind tunnel data are from Ref. 22 at $P_0 = 18$ MPa, and $H_0 = 20$ MJ/Kg reservoir conditions.

	Flight	WT	
U_∞	4211.35	4211.35	m/s
ρ_∞	0.00373	0.02244	kg/m^3
L	2.0	0.333	m
T_∞	273.9	1106.34	K
$T_{v\infty}$	273.9	2225.66	K
Ma	12.6	6.2	
Y_{N_2}	0.77	0.7406	
Y_N	0.0	0.000	
Y_{O_2}	0.23	0.1646	
Y_O	0.0	0.0377	
Y_{NO}	0.0	0.0571	